

Storm Surge and Sea Level Rise Impacts on Avian Biodiversity by Functional Traits: Assessment Using Adaptive Ensemble Deep Learning Models

Liying Li¹, Marcos Zuzuarregui², Junwen Bai³, Shoukun Sun⁴, Yangkang Chen⁵,
Zhe Wang¹, Daniel Fink³

Abstract

Deep learning models have demonstrated their strong capability in identifying patterns in various areas, such as finance, medicine, and disaster forecasting. In this research, deep learning models were employed to detect species distribution patterns and map the impacts of storm surge and sea level rise on the Gulf's ecosystem biodiversity. This effort was built on an existing artificial intelligence (AI) technique, Deep Reasoning Neural Networks-Multi-variate Probit Models (DRNets-MVPM), and the species distribution model, Adaptive Spatial Temporal Ensemble Models (AdaSTEM). A suite of species and environmental data was synthesized to model two storm surge and sea level rise scenarios (Low and Intermediate-High). The deep learning approach was supported by both the biotic and abiotic niches theories through rich context, as modeled against 34 predictive variables for 332 species through deep learning. We discovered the spatial and temporal varying patterns in storm surge impacts. Spatially, storm surge at low sea level rise will shift bird species inland and cause higher density of species in distribution areas near coastal areas, potentially intensifying species competition. In comparison, storm surges with intermediate-high sea level rise scenarios will shift species ranges eastward or westward, rather than inland. By seasons, species have different vulnerability to storm surges across different months. Ensemble models have better stability and accuracy than single models at all levels including species-level, richness-level, and community-level. Our research accommodates species-specific responses, interspecies dynamics, and climate-driven habitat shifts, offering a toolset for decision-makers to respond to environmental change proactively.

¹ National Center for Ecological Analysis and Synthesis, Santa Barbara, California, United States

² University of California, Merced, California, United States

³ Cornell University, Ithaca, New York, United States

⁴ University of Idaho, Idaho Falls, Idaho, United States

⁵ University of Illinois Urbana-Champaign, Champaign, Illinois, United States

1 Introduction

Among the threats that climate change poses to ecosystems, sea level rise (SLR) and extreme storm surges have a devastating impact on coastal ecosystems. The northern Gulf of Mexico is located at the intersection of the Atlantic, Mississippi, Central, and Pacific Flyways, making it the heart of bird migration. Sea level rise (SLR) and climate change are projected to impact the Gulf's bird species assemblage (Burger, 2017). Many salt and brackish marshes may become permanently inundated due to SLR. Loss of wetlands and low-lying terrestrial ecosystems can make four out of five bird species lose their current habitat (Klingbeil et al., 2021). Furthermore, birds may not adapt to extreme events at the same level as to slow changes (Pol et al., 2010), as extreme storm surges can render islands, beaches, or salt marshes unusable for breeding or foraging birds (Daniels et al., 1993). More frequent hurricanes and storms with climate change can flood nests, eggs, and chicks, which is detrimental to reproductive success.

Previous studies already suggest that habitats and coastal birds' species assemblages will shift considerably over the coming decades in the Gulf of Mexico (Day et al., 2008; Forbes and Dunton, 2006; Greenberg et al., 2006). However, there are knowledge gaps regarding the ecological impacts of storm surges on species-level population changes by seasons for a wide range of avian species and relevant shifts in community composition with SLR. Existing methods exhibit significant uncertainty in bird population projections (Klingbeil et al., 2021), as well as a lack of information on community composition shift and species residencies to changes in a community.

Although expected overall species loss due to extreme events, species assemblages affects biodiversity residencies. For example, censuses of birds in coastal marshes of Alabama and Mississippi found that SLR and landward changes in habitat and salinity will lead to population increases in Seaside hawks and clamber Rails and decreases in Least Bittern (Rush et al., 2009). Therefore, accurate predictions of where and how biodiversity will be impacted based on whole assemblage of local species can help prioritize conservation resources, guide adaptive management strategies for preservation biodiversity under various SLR scenarios proposed by the IPCC (Pierce et al., 2018). Species distribution modeling that only projects the responses of a few species cannot comprehensively reflect avian biodiversity responses to the ever-changing environment(Ovaskainen et al., 2017; Warton et al., 2015). We need to jointly model multiple species occurrences to account for ecological interactions and shared responses to environmental change.

Deep learning models are well-suited for extending to multi-output settings in Joint SDMs (Bai et al., 2020, 2022) because of their computation speed, capability of capturing complex non-linear interspecific interactions (Chen et al., 2016; Tang et al., 2018), and handling sparse data (Hirn et al., 2024) data with scalable computation (Chen, 2020). Modeling complex ecological phenomena, including species distribution modeling (Dinnage, 2024) requires such ability in handling high-dimensional, multi-modal data, and complex nonlinear relationships (Suzuki et al., 2016), as often observed in ecological data (Christin et al., 2019). Interpretability can be improved through embedding analysis, making complex models ecologically insightful. We used deep reasoning neural networks (Chen et al., 2021) for the multivariate probit model (Lesaffre and Molenberghs, 1991) (DRNets-MVPM) to achieve the research objective of predicting storm surge impacts on avian biodiversity by different sea level rise

scenarios and inform conservation actions.

DRNets-MVPMs have been tested as suitable for predicting joint species occurrences with better performance than some of the best joint SDMs recognized in the literature (Davis et al., 2023; Norberg et al., 2019). This model also bridges the gap that existing deep learning SDMs often fail to be probabilistic models (Dinnage, 2024). Probabilistic models are generally considered superior to deterministic models as ecological observations are zero-inflated and have incomplete detection. Species that are not detected can represent a low occurrence probability rather than absolute absence. Additionally, not all factors that impact species distribution can be observed, as real-world entities do not exist in a vacuum. Therefore, a probabilistic deep learning model provides flexibility for imperfect detections, enabling accurate predictions.

To handle non-stationary spatial and temporal bias and capture seasonal species dynamics and variation in impact levels of storm surge by seasons, DRNets-MVPMs were grouped in the AdaSTEM framework (Fink et al., 2020) to predict species distribution with spatial and temporal sub-models. An identical static version of DRNets-MVPM was used to compare its performance with that of the adaptive dynamic approach, AdaSTEM DRNets-MVPM. A total of 332 species were modeled simultaneously against 34 predictive variables to predict storm surge impacts on bird species distribution under both Low (+0.2m from the c. 2000 mean sea level (MSL) by 2100) and Intermediate-High (+1.2m from MSL by 2100) sea level rise scenarios. The outputs of species distribution were then merged with species functional traits and analyzed to determine how morphological features, foraging behavior, and migration patterns affect birds' resilience to storm surge impacts. We found the bird species will be impacted by storm surges with different severity across the different storm occurrence months. When sea level rise reached intermediate high level, most birds leave the impacted areas for survival.

2 Methods

2.1 Spatial and temporal ensemble model with AdaSTEM

AdaSTEM has been applied to a wide range of studies that assess how species distribution patterns change across space (Fink et al., 2023), time (Fink et al., 2020), and various anthropogenic (La Sorte et al., 2022) and environmental factors (Cohen et al., 2020). These models reveal significant improvements in capturing species' habitat preferences (Li et al., 2025a,b) and migration patterns (Haas et al., 2022) compared to static models (Chen et al., 2024). The integration of temporal temporally dynamic factors (e.g., climate variability and migration stages) can forecast invasive species risk (Formoso-Freire et al., 2023), range shifts risks of migratory species (La Sorte et al., 2017), and species movement dynamics (Ruiz-Gutierrez et al., 2021), which traditional models often inadequately capture Soriano-Redondo et al. (2019). Ensemble models that adapt to non-stationary spatiotemporal heterogeneity can also address temporal and spatial observation biases in citizen science data (Fink et al., 2010). More importantly, they improve prediction performance by avoiding overfitting across a large spatial scale (de Rivera et al., 2019). Compared to static models, AdaSTEM has the advantages of predictive accuracy and computational efficiency (Ward et al., 2022). Al-

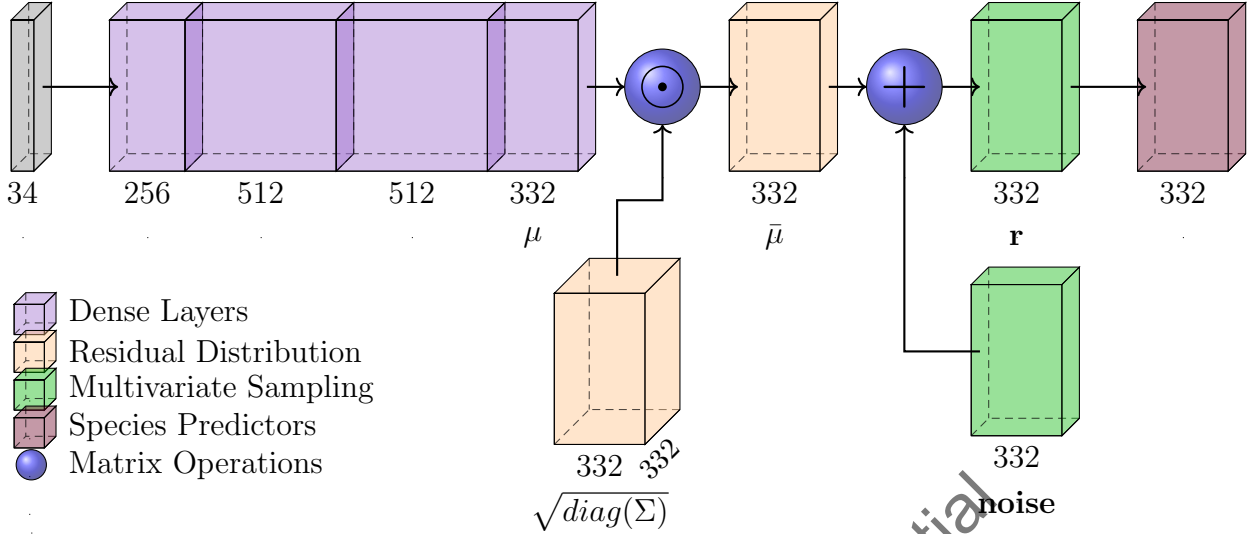


Figure 1: Model architecture of our residual, probabilistic network.

though static models can perform well under certain data conditions, particularly when spatial coverage is limited or data are clumped (Redding et al., 2017). The accuracy gains in AdaSTEM benefit predictions for nomadic or range-expanding species the most (Andrew and Fox, 2020). Ensemble and adaptive partitioning methods can be computationally intensive, but are suitable for computational parallelization (Chen, 2020), which reduces training time. The StemFlow package (Chen et al., 2024) was acquired and modified to perform the AdaSTEM. The 10-year eBird observation data were first grouped into each of the 12 months based on the observation day of the year and then were partitioned by the modified StemFlow package into spatial boxes (Fink et al., 2020) that dynamically adapt to observation data densities across space (minimum 500 samples per box). The spatial boxes were also constrained to be no larger than 5° longitude \times 5° latitude and no smaller than 1° longitude \times 1° latitude by implementing forced splitting or aggregation, respectively. The number of spatial boxes varies between months and dynamically adjusts to the available observations for each month. The temporal dynamic is essential for predicting the seasonal dynamics of species movement (Andrew and Fox, 2020). The modified StemFlow code can be found in the code availability session.

2.2 Deep Reasoning Networks for Multivariate Probit Models

A deep reasoning neural network (Chen et al., 2021) for our multi-variate probit model is a deep probabilistic neural network for joint species distribution modeling (JSDM) (Norberg et al., 2019) that captures both species–environment relationships and interspecies dependencies (Chen et al., 2016). Coupling biotic and abiotic factors fills the gaps in the incomplete characterization of real-world scenarios of predation and competition, which also influence distribution, a factor that traditional algorithms frequently overlook. However, at the local scale, they include information about biotic variables (Barlett et al., 2024). In our model, environmental features are first passed through multi-layer perceptron of sizes 256, 512, and 512 for feature extraction, activated using rectified linear unit (ReLU) and regularized with

an L2 penalty of $1e^{-5}$ weight decay. The final layer of feature embedding outputs a species-specific mean vector μ , representing the species-specific environmental responses. To handle species correlations and uncertainty not explained by μ , a learned low-rank latent residual covariance structure was introduced in DRNets-MVPM. This residual structure is represented by a learnable square root matrix $B \in R^{S \times Z}$, which models inter-species dependencies. By combining this residual structure with a diagonal identity matrix I , parameterized by Z (number of independent variables: 20), the model ensures that the final covariance matrix is positive semi-definite (Zhang et al., 2020). This structure enables the model to capture biologically meaningful residual co-occurrence patterns, such as species that often co-occur together beyond what environmental variables alone can explain. This approach is inspired by latent factor models commonly used in JSDMs (Warton et al., 2015; Hui et al., 2013). We normalize the mean environmental embedding μ with the square root of the Σ diagonal to ensure the scale of the residual mean aligns with the scale of uncertainty encoded in the covariance matrix, $\bar{\mu} = \mu \odot \sqrt{diag(\Sigma)}$ with $\Sigma = BB^T + I$.

There are two key steps in estimating species presence probabilities from the latent variable samples of environmental embedding μ and species embedding Σ . One is sampling noise from a standard normal; the other is transforming it via the learned mean and covariance to get realistic samples (Kingma & Welling, 2013). Monte Carlo sampling from a multivariate Gaussian distribution ($N(\bar{\mu}, \Sigma)$) was used for sampling residuals, and the sigmoid function was used to retrieve the probability of occurrence from the latent variable matrix. The sigmoid function is a fast and stable alternative for computing the probability of occurrence ϕ to the Cumulative Density Function (CDF), and it preserves differentiability, allowing backpropagation to pass through this probabilistic layer. The stochasticity of the model by treating embeddings as a standard distribution incorporates uncertainty (via sampling). Approximated presence probability was used to enable efficient training by minimizing a composite loss including negative log-likelihood (NLL), approximate cross-entropy, and L2 loss.

Models were trained using a 500-sample mini-batch and a maximum of 100 epochs. The learning rate is $1e^{-3}$, with a decay ratio of 0.5 and three decays. Detailed functional model representations can be found in Figure 1 and Chen et al. (2016). The model code is provided in the Code Availability section. Instead of modeling each binary response directly, the multivariate probit model (Lesaffre and Molenberghs, 1991) assumes that an underlying latent continuous variable determines each binary outcome. These latent variables are modeled jointly using a multivariate normal distribution, which enables correlations among the outcomes. For range prediction, we converted the occurrence probability to presence/absence based on the Minimum Difference Threshold (MDT) criteria, which involves minimizing the difference between sensitivity (true positive) and specificity (true negative). MDT criteria have been proven as superior to other criteria, such as the 0.5T criteria (> 0.5 presence, < 0.5 absence) in predicting presence, particularly when the prevalence of presence is low (Jiménez-Valverde and Lobo, 2007). MDT criteria are implemented by looping through the threshold value from 0 to 1, searching for the threshold that minimizes the difference between the sensitivity and specificity metric for each species in each sub-model of the spatial boxes.

2.3 Species and environmental variables

eBird data (Sullivan et al., 2009) from 2015 to 2024 were acquired within the northern Gulf of Mexico coast, including the southeastern parishes of Louisiana, the coastal counties of Mississippi and Alabama, and the western counties of the Florida panhandle. The data version used in this study was the 2025 eBird Reference Dataset, and 10 years of observation were merged for data augmentation in AI model training. Checklists of all species were summarized into a table of all species observations, with each shared locality ID represented as a single row in the table, resulting in 408,338 entries (rows) including 448 species. Species with fewer than 100 occurrences across all entries and rows with only absence were removed, leaving 332 species with 404,058 data entries for subsequent model training. Environmental predictors include both ancillary geographical information, such as digital elevation, orientation, and slope, as well as environmental variables, including temperature (Bio1 & Bio7), land use classes, biomass concentration, and chlorophyll concentration. Land cover is represented by the proportions of each land cover class in a 3×3 km area around each checklist. The consideration of biomass and chlorophyll concentration underscores the importance of including the primary productivity of the ecosystem. Our innovation is a merge between both land-based and oceanic environmental variables to create a consistent prediction that covers the coastline. Terrestrial biomass was obtained from the GEDI L4B Gridded Aboveground Biomass Density (Bubayah., 2023). SUOMI-NPP VIIRS Level-3 Mapped Particulate Organic Carbon was used for the Ocean biomass density approximation (NASA, 2022a). Mapped Particulate Organic Carbon in the ocean (units of mg C / m³) was superimposed on the GEDI L4B Gridded Aboveground Biomass Density. Similarly, the terrestrial leaf chlorophyll content for the year 2020 was acquired from the Global Leaf Chlorophyll Content Dataset (GLCC) derived from MERIS and OLCI Satellite Data (Qian et al., 2023). The ocean chlorophyll concentration was acquired from SUOMI-NPP VIIRS Level-3 Mapped Chlorophyll, Version 2022 (NASA, 2022b). A full description of the list of 28 environmental variable data used, along with the data sources, can be found in Supplementary Information 3.6. Observation covariates were included to control the observation bias in terms of observation duration, time of the day, day of the year, year of the observation, and traveling or stationary observation. The difference in species resilience to climate change and sea level rise is analyzed by regressing predicted occurrence probability changes with different trait group features for each month across the whole year cycle with Ordinary Least Squares regression (OLS). Bird functional traits are acquired from the AVONET database (Tobias et al., 2022).

2.4 Storm surge by sea level rise scenarios

Climate change and sea level rise scenarios were created by modifying the historical prediction surface with replaced temperature and bathymetry digital elevation predictors under climate change. Projected temperatures were obtained from Bio-ORACLE (Assis et al., 2024) and WorldClim2 (Fick and Jijmans, 2017) for ocean and land, respectively, for both CMIP6 scenarios (SSP245 and SSP845) O'Neill et al. (2016). SSP245 temperatures were used for low sea level rise scenarios, and SSP845 temperatures were used for intermediate high sea level rise scenarios. Bio7 is not directly available from Bio-ORACLE; therefore, we calculated the Bio7 mean temperature range for oceanic areas by using the difference

between the maximum and minimum sea surface temperatures. The simulated maximum of maximum (MOM) storm surge water surface elevation (Bilskie et al., 2016) was acquired and used to modify the historical bathymetry digital elevation. SWAN+ADCIRC (Simulating Waves Nearshore+ADvanced CIRCulation) was utilized in Bilskie et al. (2016) to predict water surface elevation with storm surge by different sea level rise scenarios. The mean sea level rise bathymetry elevation equals the historical mean bathymetry elevation minus the predicted mean water surface elevation of inundation. The standard deviation of sea level rise bathymetry elevation equals the historical bathymetry elevation plus the standard deviation in predicted inundation water surface elevation, assuming the storm surge will increase the variation in water depths. We also modified the land cover class of water by revising the historical land cover classes of water based on whether the land is inundated. If land is inundated (the predicted mean water surface elevation of inundation is not zero), water cover is 1, and the other land cover classes are 0.

We predicted species occurrence probability and ranges under both historical and SLR scenarios. The species occurrence probability change was calculated by deducting sea level rise species occurrence probability by historical occurrence probability location by location. If the historical occurrence probability of a species at a location is less than 1%, we set the occurrence probability to NA to avoid infinitely large proportional change results. We selected the species without NA values in probability change across the study area and plotted them in spatial maps. Additional species occurrence probability change maps are available in the data availability repository).

3 Results

3.1 Storm surge impacts on the occurrence probability and range

Historically, the wetland habitat along the northern Gulf of Mexico coast has been a shifting mosaic of changing elevation and salinity gradients, resulting in shifts in vegetation species and patterns that confine birds' nesting and breeding locations (Burger, 2017). Past model projections of sea level rise over the next century and beyond may shift the northern Gulf of Mexico coastal environments into a new equilibrium regime (Donoghue, 2011). We uncovered how storm surges that invade the shoreline are going to shift bird community and species in a spatial and temporal dynamic manner with different sea level rise scenarios (Figure 2 and 3). DRNet-DVPM explicitly maps species-specific changes in occurrence probability, revealing pronounced seasonal variation in storm-surge impacts on bird occurrence that differs across species. For example, in Figure 2, in the Low-level SLR scenario (SSP2-4.5), we highlighted Laughing Gull, Great Egret, and Osprey: Laughing Gull exhibits the weakest seasonal variation in storm surge effects, whereas Great Egret and Osprey show much stronger, seasonally structured occurrence probability impacts by storm surges. That is, if the storm surge had happened later in the year, in November, it would have a more pronounced reorganization of Osprey habitat than if it had happened in summer. In the fall and winter, when post-breeding movements dominate, Osprey displays some of its largest negative changes relative to the historical scenario along exposed headlands and barrier shorelines. Even inland areas in Louisiana that were not impacted by simulated storm surge showed a pronounced de-

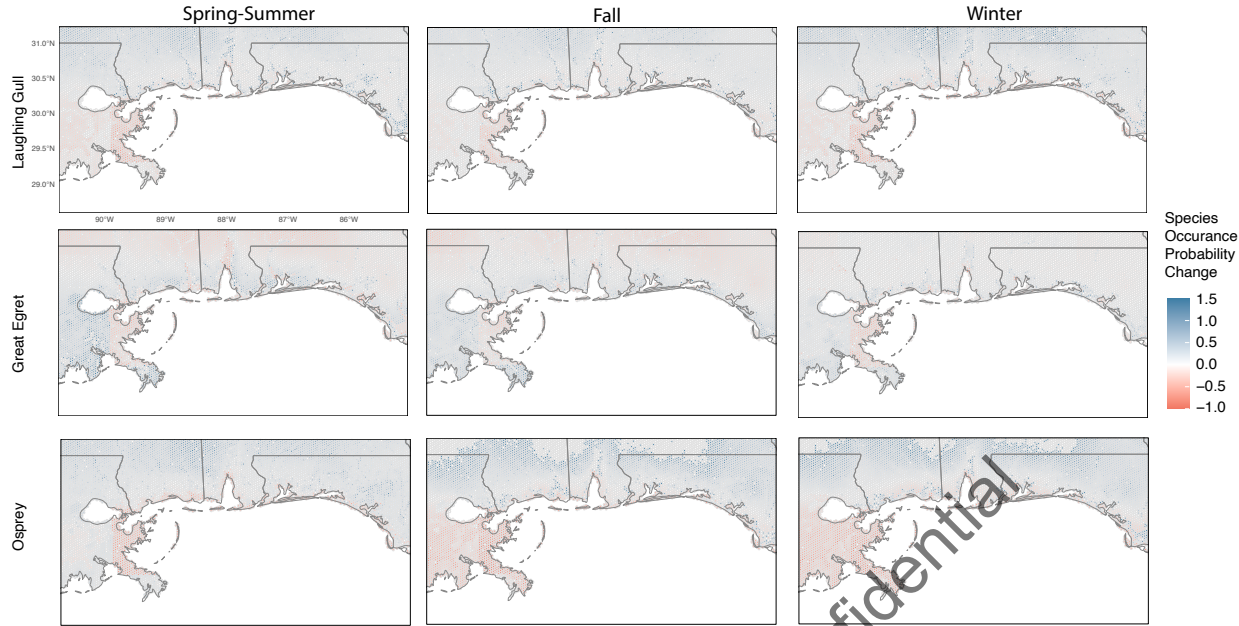


Figure 2: Species occurrence probability change impacted by storm surge in different seasons expressed as a proportion of their value in 2000, under RCP245 climate and Low-level (0.2m by 2100) sea level rise scenarios,

crease, as represented in the map units in Red. For the Great Egret, however, the impacts of seasonality are the opposite. If a storm surge had occurred in summer, the occurrence probability would have been reduced by more than 50% in both coastal and inland areas. In summer, the clear dividing line in Louisiana's Atchafalaya Basin for all three species maps, shows the boundary of storm surge simulation used in this study (Supplementary Materials S1 Figure S4).

Spatially, Great Egret tends to lose occurrence probability in interior estuaries and marsh systems, where storm surges deepen normally shallow foraging zones in tidal creeks and inner marshes, reducing access to suitable depths. Tidal creek confluences, bay-head deltas, and flooded marsh ponds serve as refugee when exposed outer marsh fringes lose habitat suitability to them under repeated fall surges. Different than Great Egret, Laughing Gull and Osprey lost their habitat sustainability along open beaches and low-lying nesting shorelines, where repeated inundation reduces nesting suitability. Osprey's coastal foraging is sensitive to surge in all seasons, except in winter river mouths and estuarine channels across the coast showed increases in Osprey habitat suitability where surge-driven flows aggregate prey. Similarly, Laughing Gull exhibits some clear summer gains along barrier-island and beach systems, where surge-driven mixing over sandbars and shoals elevates occurrence probability.

When sea level rise is at an intermediate-high level (SSP5-8.5), all three species saw a different migrating pattern of escaping the storm surge hazards than the low-level scenarios (Figure 3). Species shift either eastward (Laughing Gull and Osprey) or westward (Great Egret). The most vulnerable season for Laughing Gull and Great Egret is Summer, and for Osprey is still in Winter. The most resilient season for Laughing Gull is Fall, for Great Egret

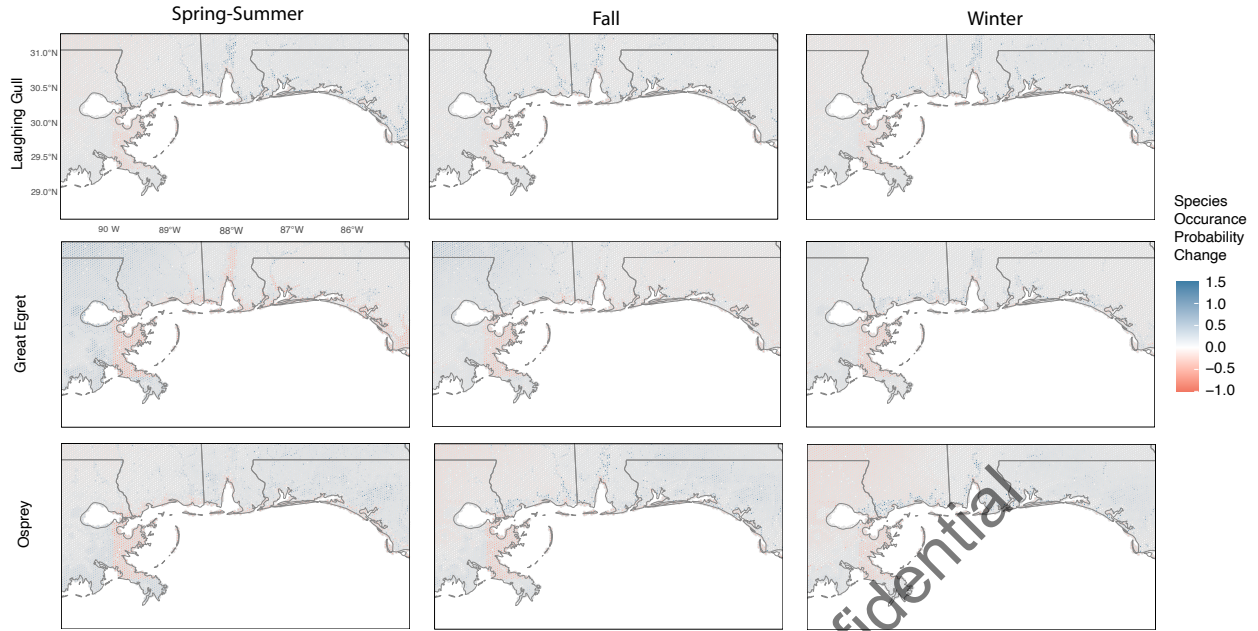


Figure 3: Species occurrence probability change impacted by storm surge in different seasons expressed as a proportion of their value in 2000, under the RCP585 climate and intermediate high level (1.2m increase by 2100) sea level rise scenario

is winter, and lastly for Osprey it is summer.

Based on species occurrence probability, we applied the MDT criterion (see Methods) to convert occurrence probabilities to binary presence/absence and produced species range maps for the three scenarios (historical, Low SLR, and Intermediate–High SLR; Fig. 4). Great Egret and Osprey were retained in this figure to allow direct comparison with their probability surfaces in Figure 3, while Laughing Gull was omitted because its range-shift pattern closely resembles that of Osprey. We additionally included two species with highly distinctive morphology and high observation rates—Blue Jay and Brown Pelican—to illustrate contrasting, well-supported range-shift responses. The resulting maps reveal several clear patterns. We observed Blue Jays flying from inland to flooded areas. Their historical ranges concentrated inland but with storm surges increasing presence was observed in low-lying, surge-affected areas, consistent with a generalist that can exploit newly inundated or edge habitats. In contrast, Brown Pelican range didn't shift as apparently as other species in the low sea level rise scenario, but contract sharply under Intermediate–High SLR: pelicans were wiped out along the Gulf shorelines of Mississippi, Alabama, and Florida, with remaining presence concentrated along the Louisiana coast and in inland areas that lie outside the simulated storm-surge footprint. Great Egret and Osprey display a broadly similar contraction in their ranges, but are less coastal-resilient than Brown Pelican. Even under Low SLR, their coastal ranges are largely eliminated from the coast, persisting mainly in parts of coastal Louisiana and inland habitat refugee. Under Intermediate–High SLR, Great Egret and Osprey disappears almost entirely from surge-impacted cells, indicating a pronounced loss of suitable coastal habitat. Together, these examples show that storm surge interacting with sea-level rise produces strongly species-specific range responses, with some

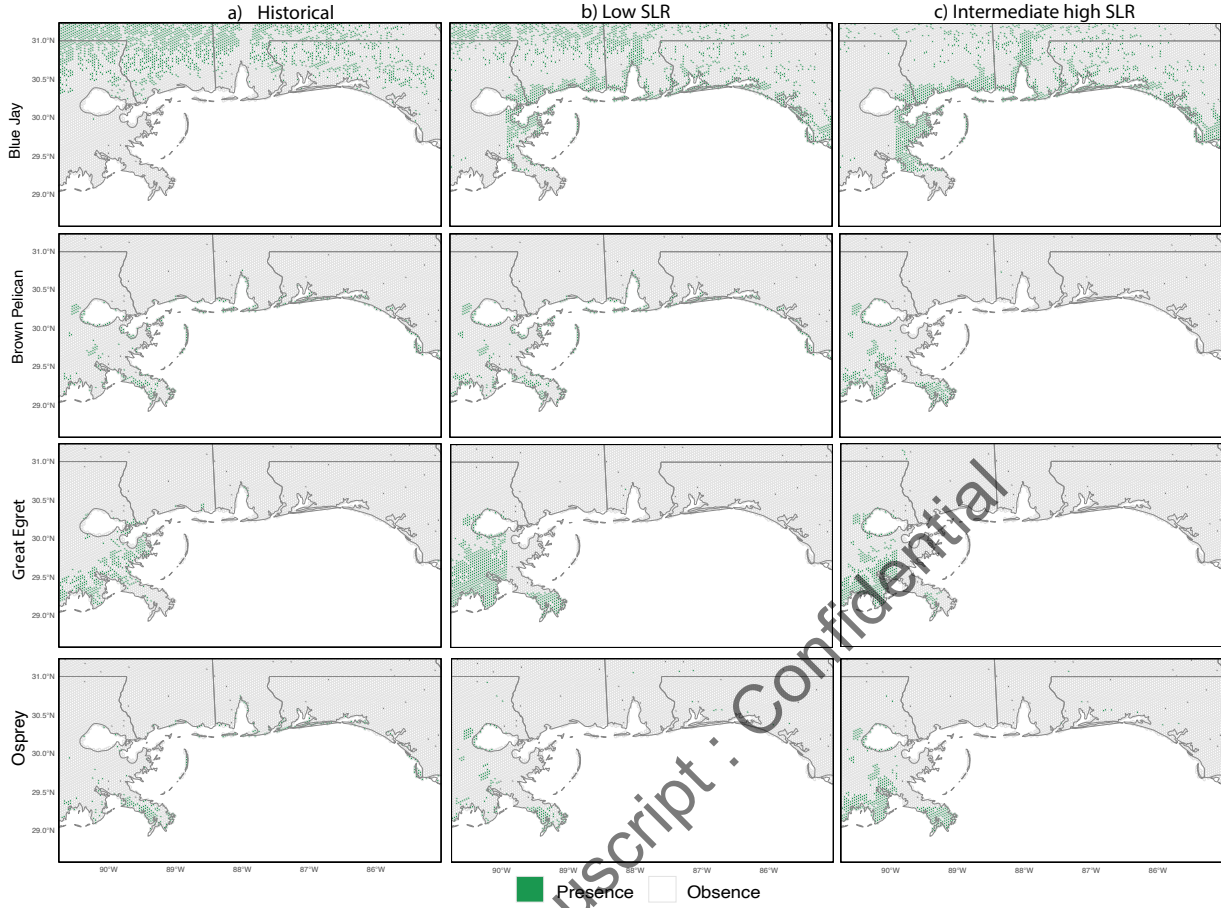


Figure 4: Species range shifts across sea-level rise scenarios, shown from left to right as (a) historical, (b) low sea-level rise, and (c) intermediate–high sea-level rise.

generalists tracking new flooded habitats and many coastal specialists losing large portions of their historical Gulf coastline ranges.

3.2 Storm surge impacts on the community richness

We mapped the richness and richness changes of 332 modeled bird species across the entire study region and found that how far and how strongly a single storm surge erodes coastal bird richness depends critically on the long-term sea-level trajectory (Figure 5 and Figure 6). Under current (historical) climate and sea-level conditions, the northern Gulf coast supports exceptionally high September richness (Figure 5). The Gulf is the heart of four North American flyways, hosting semiaquatic birds, and all land bird species have been reported either on Gulf islands or crossing its waters. Approximately 44% of reported species are aquatic, 27% are marine, and 29% are terrestrial (Gallardo et al., 2009). Under historical climate and sea level, a continuous band of high species richness hugs the northern Gulf of Mexico, especially along the southeastern parishes of Louisiana, the coastal counties of Mississippi and Alabama, and the western Florida Panhandle. Richness drops off rapidly inland: once you leave the immediate coastal wetlands, estuaries, and barrier islands, colors become

darker (lower richness), although bright spots persist along major estuaries and river channels. Overall, September bird diversity is tightly packed into low-lying coastal habitats, with inland richness largely confined to corridors that track tidal rivers and estuarine networks.

Under Low SLR with a September storm surge, the main impact zone is confined to a thin coastal strip. Bright coastal pixels along Mississippi, Alabama, and the western Florida Panhandle become slightly brighter overall (more active species). Along the shoreline of Lake Pontchartrain in Louisiana, many species tracked surge-driven habitat changes. In southern Louisiana, commonly known as Atchafalaya Basin or Bayou Country, responses are spatially heterogeneous: some areas darken while others brighten, reflecting the fact that the simulated storms have specific, localized impact footprints. Notably, the southern tip of the Atchafalaya Basin emerges as one of the hottest bird-diversity spots, sitting just outside the main impacted areas by simulated storms and therefore concentrating species displaced from elsewhere. Inland mostly remains bright, and in several places coastal birds pushed off inundated habitats are redistributed into slightly higher, just-inland areas, leading to local inland brightening (small richness gains). Under Intermediate–High SLR, with the same September surge, the impact footprint expands both inland and along the shore. Areas that were bright and relatively safe in the Low scenario—especially low coastal plains and inner estuary margins—become noticeably darker, indicating substantial richness losses. Instead of a broad inland band of high richness, the landscape breaks up into isolated bright “islands” of diversity, and the entire impact zone within the Atchafalaya Basin becomes dark. The refugee pattern shifts: in many stretches, only a very narrow strip right at the shoreline retains high richness (for example, along the crests of some barrier islands or slightly elevated coastal ridges), while the adjacent inland and shoreline cells are much darker.

In the richness change map by seasons (Figure 5), we found that storm surges have seasonally varying impacts on habitat suitability. Under Low SLR (SSP2–4.5), in both summer and fall storms, the strongest richness changes remain tightly coastal: most large negative bins hug the immediate shoreline—barrier islands, outer marshes, and bay mouths. Just landward of this fringe, a distinct purple loss band appears. These cells are primarily inner-bay marshes, low coastal plains, and highly modified transition zones, where surge water tends to pile up and linger, producing longer, deeper inundation than on higher inland ground. This band often mixes dredged canals, levees, roads, drained wetlands, and low agricultural or developed areas. These landscapes are already habitat-poor; when the surge arrives, they do not gain much new usable habitat, but they lose what little structure they had. As a result, the most exposed shoreline (e.g., inlet shoals) can still host many birds immediately after the storm—prey is concentrated and coastal specialists persist there—while the inner, higher ground functions as refugee, where displaced birds find trees, fields, and patchy wetlands. The middle band is too wet and disturbed for many species and, therefore, appears as a clear strip of richness loss between the coast and inland locations. In summer, most inland changes are small (± 1 – 5 or ± 5 – 25 species), and many cells show little to no change, indicating that the bulk of inland richness structure survives the storm with only modest reshuffling. Patches of positive change inland of impacted coasts suggest that some birds are temporarily displaced upslope or up-estuary, creating local inland brightening rather than uniform loss. The fall panel shows a similar coastal band of impact, but the loss band is squeezed closer to the shoreline, reflecting different seasonal communities. The most directly exposed shoreline segments show a wider band of strong losses, while the inner loss band

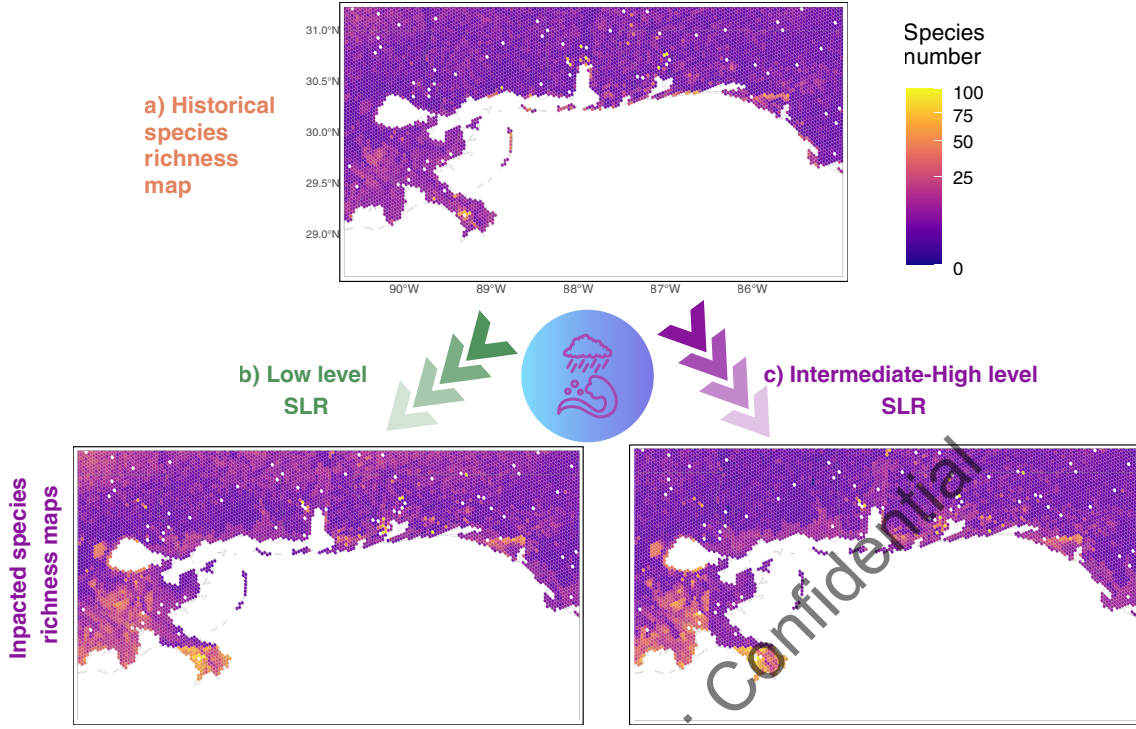


Figure 5: Species richness maps in September based on 332 modeled species under (a) historical climate and sea-level conditions in 2020, and maps of richness impacted by a September storm surge under two sea-level rise scenarios: (b) Low, corresponding to SSP2-4.5 climate with 0.2 m mean sea-level rise by 2100; and (c) Intermediate-High, corresponding to SSP5-8.5 climate with 1.2 m mean sea-level rise by 2100.

narrows. Along estuary margins and bay interiors, there are more mixed patches of gain and loss, consistent with fall migration: some cells lose tens of species while adjacent cells gain, as migrants redistribute along the coast. Most inland areas, however, continue to function as refugee and buffers even in fall.

Under Intermediate-High SLR, the scale and depth of impact expand nonlinearly: the same type of surge event affects much more extensive inland areas and many more species. Both summer and fall storms carve out a much wider and more continuous band of loss, and the difference between seasons is now mainly in intensity and exact spatial placement, rather than in whether inland areas are safe; many inland areas are no longer effective species-diversity refugia. Segments that appeared to be stable inland refugia under the Low SLR scenario now fall into mid-high loss bins, indicating that higher mean sea level allows the same storm to propagate farther inland. In summer, the impact band thickens and shifts inland: areas that were only lightly affected under Low SLR now show losses of 5 to 25 species, especially in low-lying coastal plains and inner estuary margins. Scattered positive hotspots persist but are more isolated, forming small green "islands" embedded within a broader field of losses. In fall, the inland expansion of losses is even more pronounced: broad swaths of cells show -25 to -50 and -5 to 0 species, not just along the surf zone but well

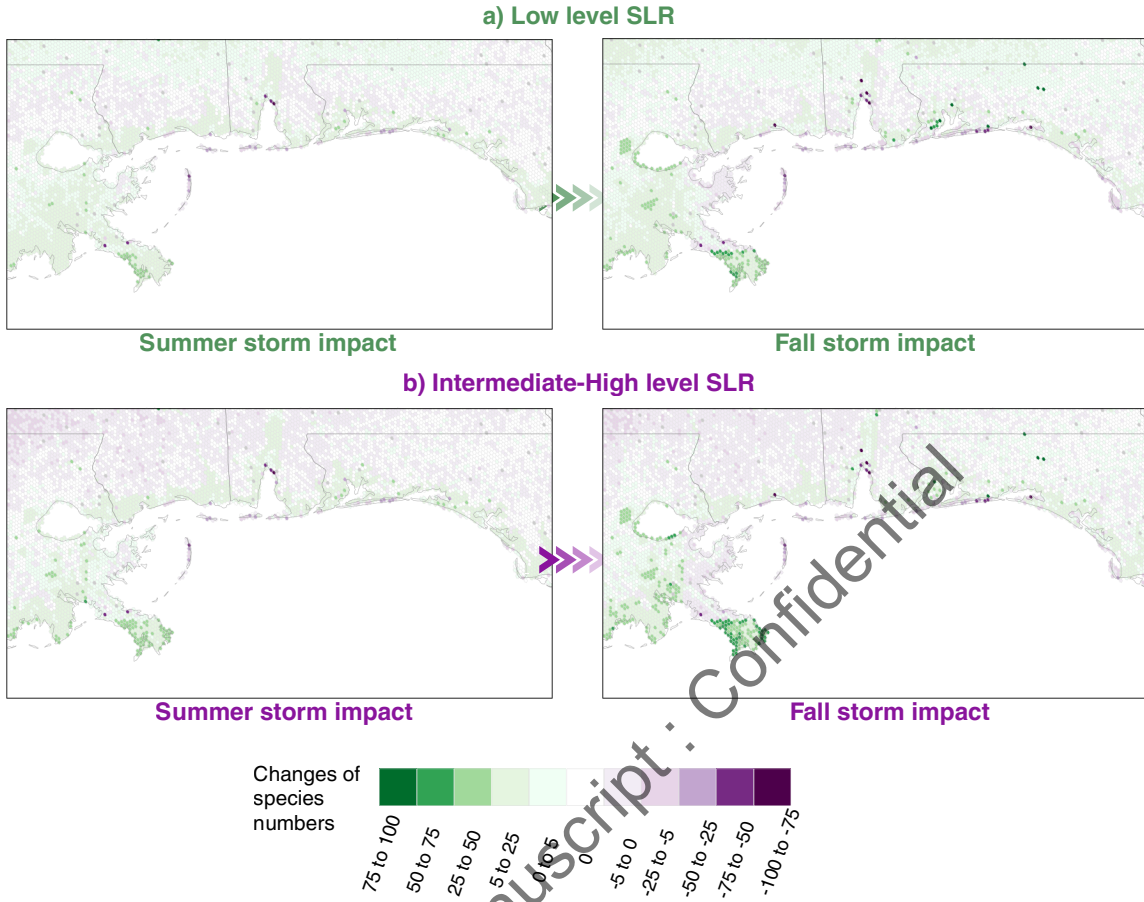


Figure 6: Species richness change, expressed as the change in number of species relative to baseline 2020 richness, caused by storm surges occurring in July (summer) and September (fall). Results are based on 332 modeled species under two sea-level rise scenarios: (a) Low, corresponding to SSP2-4.5 climate and 0.2 m mean sea-level rise by 2100; and (b) Intermediate-High, corresponding to SSP5-8.5 climate and 1.2 m mean sea-level rise by 2100.

inside estuarine and deltaic interiors. The Chandeleur Islands sadly belong to loss regions across all scenarios and seasons. The Atchafalaya Basin, which acted as a stronghold or even a gain area under Low SLR in summer, becomes largely darkened in fall under High SLR, meaning that tens of species are lost even in what used to be a seasonal hotspot. Fall migration amplifies this effect, converting much of today's high-richness coastline into an extended corridor of species loss. In addition, storm surges increase ecological pressure in parts of Louisiana and farther west that lie just outside the directly inundated zone, potentially intensifying competition for food, disrupting local communities, and propagating ecosystem-level impacts beyond the immediately flooded areas.

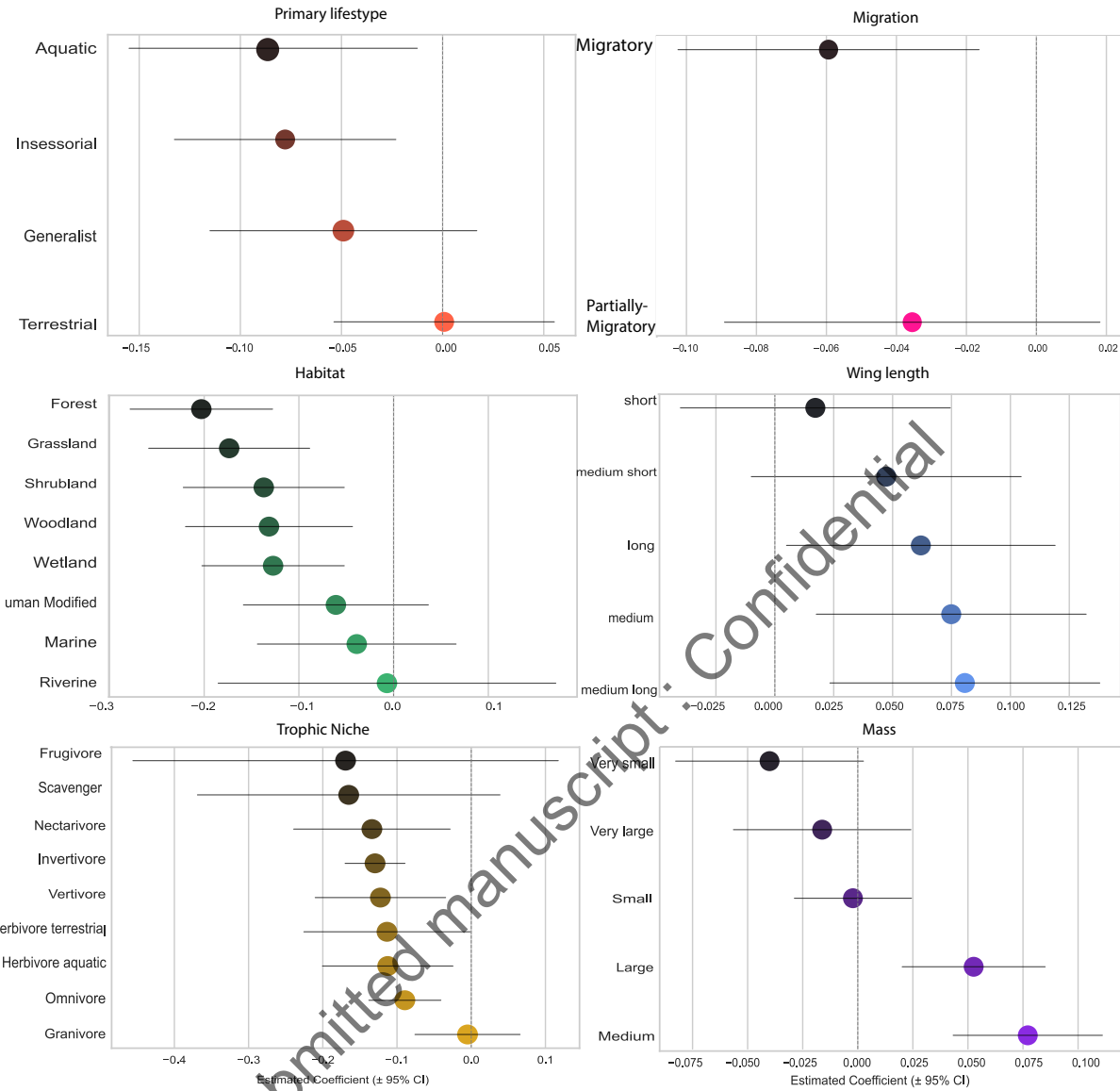


Figure 7: Effects of trait groups on species resilience to storm surge impacts in September in the intermediate-high-level sea level rise scenario represented by OLS regression coefficients

3.3 Species resilience to storm surge impacts by functional traits

We concatenated the predicted storm surge impact on species occurrence probability with the birds' trait features. The resilience of species to storm surge changes across functional trait groups was investigated and plotted using OLS regression, as described in the method section (Figure 7). If the coefficient is below zero, the further away from zero, the less resilient the trait group is to storm surge. The absolute value of the

coefficient represents how much smaller the change in occurrence probability is than the mean. For example, if the mean occurrence probability changes by 0.1, the forest bird

occurrence probability changes by -0.1 (0.1-0.2). If the coefficient value is above zero, the further away from zero, the more resilient the trait group is to storm surge. Figure 6 shows ordered trait groups from less resilient to more resilient from left to right for each trait category. For a continuous trait category, trait values were categorized into 5 groups based on quantiles, as shown in the plot for the Mass and Wind Length traits. Overall, a partially migratory bird is more resilient than a migratory bird. Medium-sized birds with medium-long wings are most resilient among different body weight and wing length groups. Understandably, this group of birds has the capacity to move a far distance faster than short-wing birds. At the same time, medium-sized body weight can allow them to travel with sufficient energy storage, while they are not as picky eaters as large-sized birds. As shown in the trophic niche trait category, the Frugivore is least resilient to storm surge, as they rely on fruits and plants that can be easily destroyed by the storm surge and may be hard to find in a different environment after escaping the impacted areas. Forest birds are the least resilient in storm surge (Figure 6), as forest habitat is slower to recover from devastating disasters than other habitats. The closer to the coast and water, the more vulnerable the species is to storm surge, as shown in the Primary lifestyle

3.4 Ensemble model performance evaluation

At the species level, AdaSTEM DRNets-MVPMs have higher F1 scores than static DRNets-MVPMs (Supplementary Information Figure S1, full description of metrics can be found in Supplementary Information S2). Because F1 combines sensitivity and precision, this indicates fewer missed presences and fewer false presences across species. The AdaSTEM metrics distributions show a smooth seasonal progression across months (Figure 8), reflecting the model’s ability to track seasonal shifts in species distributions and detectability. By contrast, the static model’s scores fluctuate irregularly from month to month, and the red dots almost always sit below the AdaSTEM median, often below the lower quartile, indicating systematic under performance (Figure 8). This difference arises because AdaSTEM learns different relationships in different months via sub-models—effectively using one set of relationships when wintering waterfowl dominate, another when Neotropical migrants pass through in spring or fall, and adjusting to shifts in observation effort—whereas the static model is forced to average across all seasons and never fits any one period particularly well.

At the richness level, AdaSTEM also outperforms the static model across all months (Figure 8). Richness dissimilarity is consistently lower for AdaSTEM, showing that it more accurately reproduces the spatial pattern of richness (which cells are richer or poorer and how that pattern changes through the year). Richness calibration errors are generally smaller as well, indicating that AdaSTEM better matches the magnitude of observed richness, not just its rank order. While calibration generally improves, a few outliers in richness and community calibration highlight months and locations where communities are genuinely hard to predict — highly variable communities of mixed breeding and migratory habitat use, migration timing variations across spaces, and patchy detection of rare species. Importantly, these outliers are informative rather than random, pointing to where ecological variability exceeds even flexible models’s capacity. Richness precision is also higher under AdaSTEM, meaning fewer spurious richness gains in inappropriate locations and better capture of when and where richness peaks (e.g., migratory waves and breeding concentrations). The static

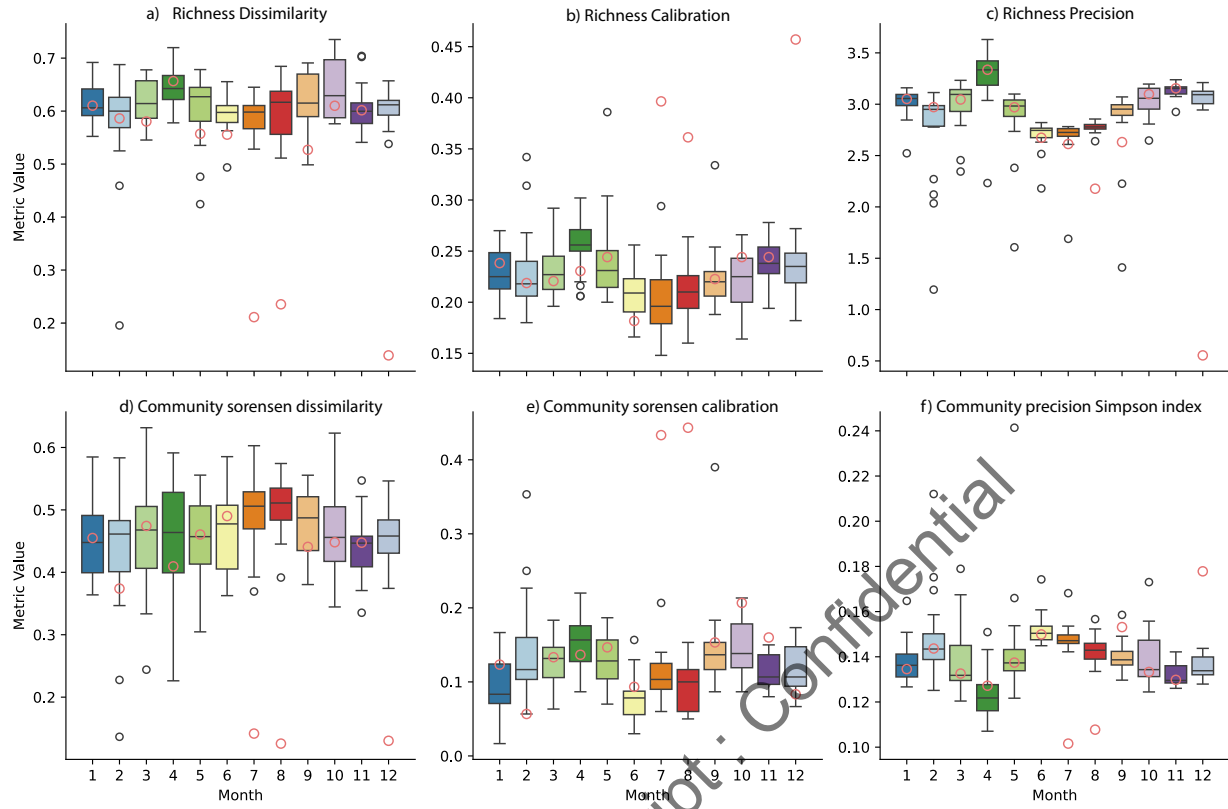


Figure 8: AdaSTEM DRNets–MVPM and static DRNets–MVPM performance for predicting species occurrence at richness and community levels across 12 months of the year. Boxplots summarize the mean, quartiles, and distribution of metrics across AdaSTEM sub-models, and red hollow circles denote the corresponding static-model metrics.

model, which lacks time-varying parameters, cannot simultaneously fit wintering hotspots in coastal marshes and lagoons, breeding hotspots in interior wetlands and forests, and the moving migratory fronts that sweep across the region.

At the community level, AdaSTEM DRNets–MVPMs again outperform static models in Sørensen dissimilarity, Sørensen calibration, and Simpson precision. Lower Sørensen dissimilarity (Community Dis Sor) and calibration demonstrate that AdaSTEM more accurately reconstructs which species co-occur in which places, and how these assemblages reorganize seasonally. Higher Simpson precision shows that the dominant species and major community structure, as well as marine–coastal marsh–inland forest gradients, are better captured by the dynamic framework. Error distributions also carry a clear ecological signal: community composition is easiest to model in more stable seasons (core winter or core breeding), when AdaSTEM errors are low and tightly clustered; they are largest and most variable in transitional months (spring and fall migration), when communities are literally in motion. The static model performs worst precisely in these dynamic periods, with red dots often near or above the upper tail of the AdaSTEM distributions. Taken together, Figure 8 demonstrates that stationary assumptions are inadequate for this system and that spatio-temporal partitioning in AdaSTEM is doing meaningful work: different sub-models specialize in different

seasonal regimes and spatial neighborhoods, and their aggregation yields better calibration, lower dissimilarity, and higher precision from individual species to whole communities.

4 Conclusion

Gulf coastal ecosystems face intensifying threats from climate change, yet conservation efforts are often constrained by limited foresight into how biodiversity will respond. This research advances the integration of deep learning into ecological forecasting by developing an ecologically informed and computationally scalable framework to model the impacts of storm surge and sea level rise on coastal avian biodiversity. By combining Deep Reasoning Neural Networks–Multivariate Probit Models (DRNets-MVPM) with Adaptive Spatiotemporal Ensemble Models (AdaSTEM), we produced high-resolution species occurrence predictions for 332 bird species across diverse spatial and environmental gradients using adaptive ensemble learning of deep neural networks. The resulting model captures both species-specific and community-wide ecological responses with improved accuracy, stability, and calibration compared to traditional static models.

The impact assessment using adaptive ensemble DRNet-MVPM accounts for seasonal dynamics in species responses to storm surges with different sea levels—highlighting inland compression of species under low sea level rise, and east–west range shifts under Intermediate-high scenarios, demonstrate the model’s ability to resolve complex climate–biodiversity relationships at multiple ecological levels. Refugia planning must be adapted to changes in sea levels and season-aware: areas that look safe under Low SLR in summer may no longer function as refugee under High SLR in fall. Implications for conservation is that as richness is squeezed into a narrower, fragmented set of high-richness cells, especially under High SLR, species are forced into fewer shared refuges, increasing potential for competition and community disruption. Our study areas, like many other conservation focused areas, are important habitats to wildlife and biodiversity. They sits at the intersection of four major bird flyways, the loss of inland refugee raises the risk of flyway-scale bottlenecks: fewer safe, high-richness stopover and staging sites for large numbers of migrants in both summer and fall.

Critically, it was revealed that species’ functional traits strongly modulate their resilience to storm surge. Using regression-based trait analysis, we identify that partially migratory birds, medium-sized birds with medium to long wings, and generalist foragers are among the most resilient groups. In contrast, frugivorous, forest-dependent species, and those with coastal or aquatic primary lifestyles are particularly vulnerable. This reflects a combination of mobility, energy demands, dietary flexibility, and the potential for habitat recovery. By connecting predicted range shifts with ecological traits, our model offers a mechanistic lens into species’ residencies to storm surges by seasons as constrained by their life-history strategies.

These findings offer a significant methodological advancement, demonstrating that deep learning can be ecologically interpretable, while scaling effectively across different species, functional groups, regions (across the northeastern coast of Gulf), and environmental gradients (current and sea-level-rise conditions). Beyond methodological innovation, this work provides a practical tool for informing proactive and adaptive conservation strategies in

coastal ecosystems. By forecasting how and storm surge may reshape species habitat suitability spatially and temporally, alter community structures, and compress ecological niches, our approach equips decision-makers with forecasts about regions and species at greatest risk under different climate futures. As sea level rise and extreme weather continue to reshape ecosystems globally, scalable AI-powered frameworks like ours will be vital for aligning ecological science with climate resilience and long-term conservation planning. This study presents a novel fusion of deep learning and ecological modeling, delivering critical insights for biodiversity monitoring, forecast, and conservation planning in the face of rising seas and increasing coastal hazards.

References

- Andrew, M. E. and Fox, E. (2020). Modelling species distributions in dynamic landscapes: The importance of the temporal dimension. *Journal of Biogeography*, 47:1510–1529.
- Assis, J., Fernández Bejarano, S. J., Salazar, V. W., Schepers, L., Gouvêa, L., Fragkopoulou, E., Leclercq, F., Vanhoorne, B., Tyberghein, L., Serrão, E. A., Verbruggen, H., and De Clerck, O. (2024). Bio-oracle v3.0. pushing marine data layers to the cmip6 earth system models of climate change research. *Global Ecology and Biogeography*, 33.
- Bai, J., Kong, S., and Gomes, C. (2020). Disentangled variational autoencoder based multi-label classification with covariance-aware multivariate probit model. *Proceedings of the Twenty-Ninth International Conference on International Joint Conferences on Artificial Intelligence*.
- Bai, J., Kong, S., and Gomes, C. P. (2022). Gaussian mixture variational autoencoder with contrastive learning for multi-label classification. In *international conference on machine learning*, pages 1383–1398. PMLR.
- Barlett, T. R., Laguna, M. F., Abramson, G., Monjeau, A., and Martin, G. (2024). A new distributional model coupling environmental and biotic factors. *Ecological Modelling*, 489.
- Bilskie, M. V., Hagen, S. C., Alizad, K., Medeiros, S. C., Passeri, D. L., Needham, H. F., and Cox, A. (2016). Dynamic simulation and numerical analysis of hurricane storm surge under sea level rise with geomorphologic changes along the northern gulf of mexico. *Earth's Future*, 4:177–193.
- Burger, J. (2017). Avian Resources of the Northern Gulf of Mexico. In Ward, C. H., editor, *Habitats and Biota of the Gulf of Mexico: Before the Deepwater Horizon Oil Spill: Volume 2: Fish Resources, Fisheries, Sea Turtles, Avian Resources, Marine Mammals, Diseases and Mortalities*, pages 1353–1488. Springer, New York, NY.
- Chen, D. (2020). Dmvp-drnets/ebird_entire at v1.0 · gomes-lab/dmvp-drnets.
- Chen, D., Bai, Y., Ament, S., Zhao, W., Guevarra, D., Zhou, L., Selman, B., van Dover, R. B., Gregoire, J. M., and Gomes, C. P. (2021). Automating crystal-structure phase mapping: Combining deep learning with constraint reasoning. *Nature Machine Intelligence*.

- Chen, D., Xue, Y., Chen, S., Fink, D., and Gomes, C. (2016). Deep multi-species embedding. *Proceedings of the 26th International Joint Conference on Artificial Intelligence*.
- Chen, Y., Gu, Z., and Zhan, X. (2024). stemflow: A python package for adaptive spatio-temporal exploratory model. *Journal of Open Source Software*, 9:6158.
- Christin, S., Éric Hervet, and Lecomte, N. (2019). Applications for deep learning in ecology.
- Cohen, J. M., Fink, D., and Zuckerberg, B. (2020). Avian responses to extreme weather across functional traits and temporal scales. *Global Change Biology*, 26:4240–4250.
- Daniels, R. C., White, T. W., and Chapman, K. K. (1993). Sea-level rise: Destruction of threatened and endangered species habitat in south carolina. *Environmental Management*, 17:373–385.
- Davis, C. L., Bai, Y., Chen, D., Robinson, O., Ruiz-Gutierrez, V., Gomes, C. P., and Fink, D. (2023). Deep learning with citizen science data enables estimation of species diversity and composition at continental extents. *Ecology*, 104.
- Day, J. W., Christian, R. R., Boesch, D. M., Yáñez-Arancibia, A., Morris, J., Twilley, R. R., Naylor, L., Schaffner, L., and Stevenson, C. (2008). Consequences of climate change on the ecogeomorphology of coastal wetlands. *Estuaries and Coasts*, 31:477–491.
- de Rivera, O. R., Blangiardo, M., López-Quílez, A., and Martín-Sanz, I. (2019). Species distribution modelling through Bayesian hierarchical approach. *Theoretical Ecology*, 12(1):49–59.
- Dinnage, R. (2024). Nicheflow: Towards a foundation model for species distribution modelling.
- Donoghue, J. F. (2011). Sea-level history of the northern Gulf of Mexico coast and sea level rise scenarios for the near future. *Climatic Change*, 107(1):17–33.
- Fick, S. and Jijmans, R. (2017). Worldclim 2: new 1km spatial resolution climate surfaces for global land areas. *International Journal of Climatology*, 37:4302–4315.
- Fink, D., Auer, T., Johnston, A., Ruiz-Gutierrez, V., Hochachka, W. M., and Kelling, S. (2020). Modeling avian full annual cycle distribution and population trends with citizen science data. *Ecological Applications*, 30(3):e02056. eprint: <https://esajournals.onlinelibrary.wiley.com/doi/pdf/10.1002/eap.2056>.
- Fink, D., Hochachka, W. M., Zuckerberg, B., Winkler, D. W., Shaby, B., Munson, M. A., Hooker, G., Riedewald, M., Sheldon, D., and Kelling, S. (2010). Spatiotemporal exploratory models for broad-scale survey data. *Ecological Applications*, 20(8):2131–2147. eprint: <https://esajournals.onlinelibrary.wiley.com/doi/pdf/10.1890/09-1340.1>.
- Forbes, M. G. and Dunton, K. H. (2006). Response of a subtropical estuarine marsh to local climatic change in the southwestern gulf of mexico. *Estuaries and Coasts*, 29:1242–1254.

- Formoso-Freire, V., Barbosa, A. M., Baselga, A., and Gómez-Rodríguez, C. (2023). Predicting the spatio-temporal pattern of range expansion under lack of equilibrium with climate. *Biological Conservation*, 288.
- Gallardo, J. C., Macias, V., and Velarde, E. (2009). Birds (vertebrata: Aves) of the gulf of mexico. *Gulf of Mexico—Origins, Waters, and Biota*, pages 1321–1342.
- Greenberg, R., Maldonado, J. E., Droege, S., and McDonald, M. V. (2006). Tidal marshes: A global perspective on the evolution and conservation of their terrestrial vertebrates. *BioScience*, 56:675–685.
- Haas, E. K., Sorte, F. A. L., McCaslin, H. M., Belotti, M. C., and Horton, K. G. (2022). The correlation between ebird community science and weather surveillance radar-based estimates of migration phenology. *Global Ecology and Biogeography*, 31:2219–2230.
- Hirn, J., Sanz, V., García, J. E., Goberna, M., Montesinos-Navarro, A., Navarro-Cano, J. A., Sánchez-Martín, R., Valiente-Banuet, A., and Verdú, M. (2024). Transfer learning of species co-occurrence patterns between plant communities. *Ecological Informatics*, 83.
- Hui, F. K., Warton, D. I., Foster, S. D., and Dunstan, P. K. (2013). To mix or not to mix: comparing the predictive performance of mixture models vs. separate species distribution models. *Ecology*, 94(9):1913–1919.
- Jiménez-Valverde, A. and Lobo, J. M. (2007). Threshold criteria for conversion of probability of species presence to either-or presence-absence. *Acta Oecologica*, 31:361–369.
- Klingbeil, B. T., Cohen, J. B., Correll, M. D., Field, C. R., Hodgman, T. P., Kovach, A. I., Lentz, E. E., Olsen, B. J., Shriver, W. G., Wiest, W. A., and Elphick, C. S. (2021). High uncertainty over the future of tidal marsh birds under current sea-level rise projections. *Biodiversity and Conservation*, 30(2):431–443.
- La Sorte, F. A., Fink, D., Blancher, P. J., Rodewald, A. D., Ruiz-Gutierrez, V., Rosenberg, K. V., Hochachka, W. M., Verburg, P. H., and Kelling, S. (2017). Global change and the distributional dynamics of migratory bird populations wintering in Central America. *Global Change Biology*, 23(12):5284–5296. eprint: <https://onlinelibrary.wiley.com/doi/pdf/10.1111/gcb.13794>.
- Lesaffre, E. and Molenberghs, G. (1991). Multivariate probit analysis: A neglected procedure in medical statistics. *Statistics in Medicine*, 10:1391–1403.
- Li, L., Cole, S., Rodriguez-Flores, J. M., Hestir, E., Fink, D., Viers, J. H., Medellin-Azuara, J., Conklin, M., and Harmon, T. (2025a). Synergies between agricultural production and shorebird conservation with climate change in the central valley, California, with optimized water allocation and multi-benefit land use. *Global Change Biology*, 31.
- Li, L., Dogan, M. S., Maskey, M., Rodriguez-Flores, J. M., Vache, K. B., Cole, S., Null, S. E., Viers, J. H., Safeeq, M., Medellin-Azuara, J., and Conklin, M. (2025b). Optimized water allocation with managed groundwater recharge and prioritized wetland deliveries to

moderate human-nature water use tradeoffs under climate change. *Journal of Hydrology: Regional Studies*, 60:102496.

Norberg, A., Abrego, N., Blanchet, F. G., Adler, F. R., Anderson, B. J., Anttila, J., Araújo, M. B., Dallas, T., Dunson, D., Elith, J., Foster, S. D., Fox, R., Franklin, J., Godsoe, W., Guisan, A., O'Hara, B., Hill, N. A., Holt, R. D., Hui, F. K., Husby, M., Kålås, J. A., Lehikoinen, A., Luoto, M., Mod, H. K., Newell, G., Renner, I., Roslin, T., Soininen, J., Thuiller, W., Vanhatalo, J., Warton, D., White, M., Zimmermann, N. E., Gravel, D., and Ovaskainen, O. (2019). A comprehensive evaluation of predictive performance of 33 species distribution models at species and community levels. *Ecological Monographs*, 89.

O'Neill, B. C., Tebaldi, C., van Vuuren, D. P., Eyring, V., Friedlingstein, P., Hurtt, G., Knutti, R., Kriegler, E., Lamarque, J.-F., Lowe, J., Meehl, G. A., Moss, R., Riahi, K., and Sanderson, B. M. (2016). The Scenario Model Intercomparison Project (ScenarioMIP) for CMIP6. *Geoscientific Model Development*, 9(9):3461–3482. Publisher: Copernicus GmbH.

Ovaskainen, O., Tikhonov, G., Norberg, A., Blanchet, F. G., Duan, L., Dunson, D., Roslin, T., and Abrego, N. (2017). How to make more out of community data? a conceptual framework and its implementation as models and software. *Ecology Letters*, 20:561–576.

Pierce, D. W., Kalansky, J. F., Cayan, D. R., et al. (2018). Climate, drought, and sea level rise scenarios for California's fourth climate change assessment. *California Energy Commission and California Natural Resources Agency*.

Pol, M. V. D., Ens, B. J., Heg, D., Brouwer, L., Krol, J., Maier, M., Exo, K., Oosterbeek, K., Lok, T., Eising, C. M., and Koffijberg, K. (2010). Do changes in the frequency, magnitude and timing of extreme climatic events threaten the population viability of coastal birds? *Journal of Applied Ecology*, 47:720–730.

Qian, X., Liu, L., Chen, X., Zhang, X., Chen, S., and Sun, Q. (2023). Global leaf chlorophyll content dataset (glcc) from 2003–2012 to 2018–2020 derived from meris and olci satellite data: Algorithm and validation. *Remote Sensing*, 15.

Redding, D. W., Lucas, T. C., Blackburn, T. M., and Jones, K. E. (2017). Evaluating bayesian spatial methods for modelling species distributions with clumped and restricted occurrence data. *PLoS ONE*, 12.

Ruiz-Gutierrez, V., Bjerre, E. R., Otto, M. C., Zimmerman, G. S., Millsap, B. A., Fink, D., Stuber, E. F., Strimas-Mackey, M., and Robinson, O. J. (2021). A pathway for citizen science data to inform policy: A case study using ebird data for defining low-risk collision areas for wind energy development. *Journal of Applied Ecology*, 58:1104–1111.

Rush, S. A., Soehren, E. C., Stodola, K. W., Woodrey, M. S., and Cooper, R. J. (2009). Influence of tidal height on detection of breeding marsh birds along the northern gulf of Mexico. *The Wilson Journal of Ornithology*, 121:399–405.

Soriano-Redondo, A., Jones-Todd, C. M., Bearhop, S., Hilton, G. M., Lock, L., Stanbury, A., Votier, S. C., and Illian, J. B. (2019). Understanding species distribution in dynamic

- populations: a new approach using spatio-temporal point process models. *Ecography*, 42:1092–1102.
- Sullivan, B. L., Wood, C. L., Illiff, M. J., Bonney, R. E., Fink, D., and Kelling, S. (2009). eBird: A citizen-based bird observation network in the biological sciences. *Biological Conservation*, 142(10):2282–2292.
- Suzuki, M., Nakayama, K., and Matsuo, Y. (2016). Joint multimodal learning with deep generative models. *arXiv preprint arXiv:1611.01891*.
- Tang, L., Xue, Y., Chen, D., and Gomes, C. P. (2018). Multi-entity dependence learning with rich context via conditional variational auto-encoder. *Proceedings of the AAAI conference on artificial intelligence*.
- Tobias, J. A., Sheard, C., Pigot, A. L., Devenish, A. J. M., Yang, J., Sayol, F., Neate-Clegg, M. H. C., Alioravainen, N., Weeks, T. L., Barber, R. A., Walkden, P. A., MacGregor, H. E. A., Jones, S. E. I., Vincent, C., Phillips, A. G., Marples, N. M., Montaño-Centellas, F. A., Leandro-Silva, V., Claramunt, S., Darski, B., Freeman, B. G., Bregman, T. P., Cooney, C. R., Hughes, E. C., Capp, E. J. R., Varley, Z. K., Friedman, N. R., Korntheuer, H., Corrales-Vargas, A., Trisos, C. H., Weeks, B. C., Hanz, D. M., Töpfer, T., Bravo, G. A., Remeš, V., Nowak, L., Carneiro, L. S., Moncada R., A. J., Matysiaková, B., Baldassarre, D. T., Martínez-Salinas A., Wolfe, J. D., Chapman, P. M., Daly, B. G., Sorensen, M. C., Neu, A., Ford, M. A., Mayhew, R. J., Fabio Silveira, L., Kelly, D. J., Annorbah, N. N. D., Pollock, H. S., Grabowska-Zhang, A. M., McEntee, J. P., Carlos T. Gonzalez, J., Meneses, C. G., Muñoz, M. C., Powell, L. L., Jamie, G. A., Matthews, T. J., Johnson, O., Brito, G. R. R., Zyskowski, K., Crates, R., Harvey, M. G., Jurado Zevallos, M., Hosner, P. A., Bradfer-Lawrence, T., Maley, J. M., Stiles, F. G., Lima, H. S., Provost, K. L., Chibesa, M., Mashao, M., Howard, J. T., Mlamba, E., Chua, M. A. H., Li, B., Gómez, M. I., García, N. C., Päckert, M., Fuchs, J., Ali, J. R., Derryberry, E. P., Carlson, M. L., Urriza, R. C., Brzeski, K. E., Prawiradilaga, D. M., Rayner, M. J., Miller, E. T., Bowie, R. C. K., Lafontaine, R.-M., Scofield, R. P., Lou, Y., Somarathna, L., Lepage, D., Illif, M., Neuschulz, E. L., Templin, M., Dehling, D. M., Cooper, J. C., Pauwels, O. S. G., Analuddin, K., Fjeldså, J., Seddon, N., Sweet, P. R., DeClerck, F. A. J., Naka, L. N., Brawn, J. D., Aleixo, A., Böhning-Gaese, K., Rahbek, C., Fritz, S. A., Thomas, G. H., and Schleuning, M. (2022). AVONET: morphological, ecological and geographical data for all birds. *Ecology Letters*, 25(3):581–597. *eprint*: <https://onlinelibrary.wiley.com/doi/pdf/10.1111/ele.13898>.
- Ward, E. J., Barnett, L. A., Anderson, S. C., Commander, C. J., and Essington, T. E. (2022). Incorporating non-stationary spatial variability into dynamic species distribution models. *ICES Journal of Marine Science*, 79:2422–2429.
- Warton, D. I., Foster, S. D., De'ath, G., Stoklosa, J., and Dunstan, P. K. (2015). Model-based thinking for community ecology. *Plant Ecology*, 216:669–682.